Supplementary Information

Se-Vacancy Induced Structural Reconstruction of Iron Nickel Selenium Nanosheets for Efficient and Durable Electrocatalytic Alkaline Water and Seawater Oxidation

Wenhao Liu[1], Wei Li[1*], Zhao Liang[2*], Yufei Feng[2], Shaobo Ye[2], Chenchen Yue[2], Rui Ming[2], Xuyang Lu[2], Weiyou Yang[2] and Qing Shi[2*]

1. School of Energy and Power Engineering, Changsha University of Science & Technology, Changsha, 410014, China.

2. Institute of Micro/Nano Materials and Devices, Ningbo University of Technology, Ningbo, 315211, China.

* Corresponding author

E-mail: sq@nbut.edu.cn

DFT Calculations

Electronic and structural optimizations were performed using the Vienna Ab-initio Simulation Package (VASP) with Density Functional Theory (DFT). The Generalized Gradient Approximation (GGA) with the Perdew-Burke-Ernzerhof (PBE) functional was used to treat exchange and correlation interactions of electrons, and the D3 (BJ) dispersion correction was added to account for long-range van der Waals interactions. The projector augmented wave (PAW) method was employed to describe the interaction between the core and valence electrons. All calculations were carried out using a plane-wave basis set with an energy cutoff of 500 eV. The k-point sampling of the Brillouin zone was performed

using the Monkhorst-Pack scheme with a 2×3×1 k-point mesh in reciprocal space. The convergence criteria for structural optimization were set as 0.02 eV/Å for the force on atoms and 10-5 eV for the energy difference between two consecutive ionic steps. A vacuum layer of at least 15 Å was employed to eliminate interactions between periodic images. To account for the magnetic properties, spin-polarized calculations were performed. The initial magnetic moments were set to 4.0 μB for Fe and 2.0 μB for Ni, based on their expected high-spin states. The following four steps outline the OER process:

$$* + OH^- \rightarrow *OH + e^- \quad (1)$$

$$*OH + OH^- \rightarrow *O + H_2O + e^- \quad (2)$$

$$*O + OH^- \rightarrow *OOH + e^- \quad (3)$$

$$*OOH + OH^- \rightarrow * + O_2 + H_2O + e^- \quad (4)$$

For the OER reaction, the calculation formula for the Gibbs free energy (ΔG) at 300 K is given by $\Delta G = \Delta E + \Delta EZPE - T\Delta S$, where ΔE is the adsorption energy in the system, T is the temperature, and ΔS is the entropy adsorbed on the substrate. The vibrational analysis of the adsorbate is performed using the harmonic approximation, while the gas-phase reference molecule is treated as an ideal gas.

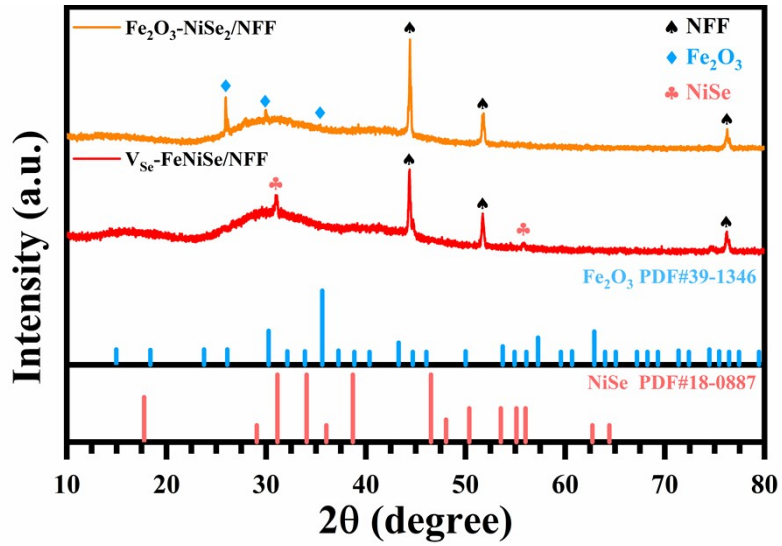

Figure S1. XRD patterns of Fe_2O_3-$NiSe_2$/NFF and V_{Se}-FeNiSe/NFF from 10 to 80 degree.

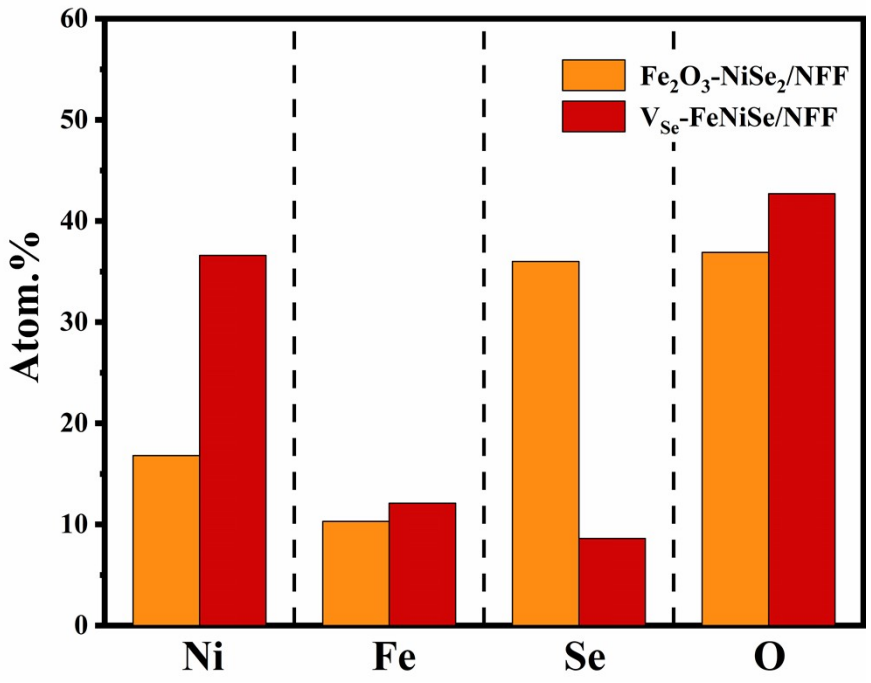

Figure S2. Atomic percentage of the elemental content in the Fe_2O_3-$NiSe_2$/NFFand V_{Se}-FeNiSe/NFF samples.

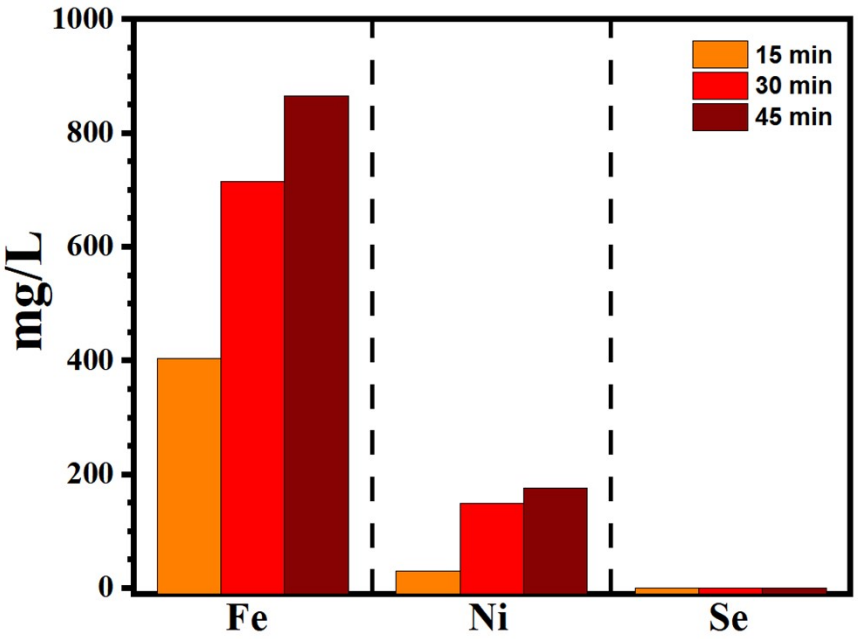

Figure S3. The atomic percentage of element contents in the etching solution at 15, 30 and 45 min.

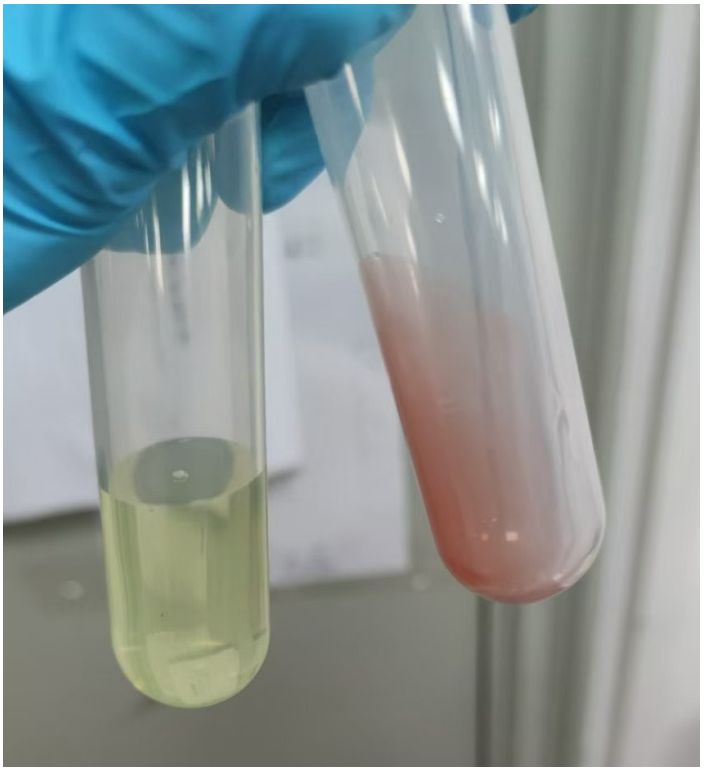

Figure S4. The macrophotograph of etching solution before and after centrifugal separation.

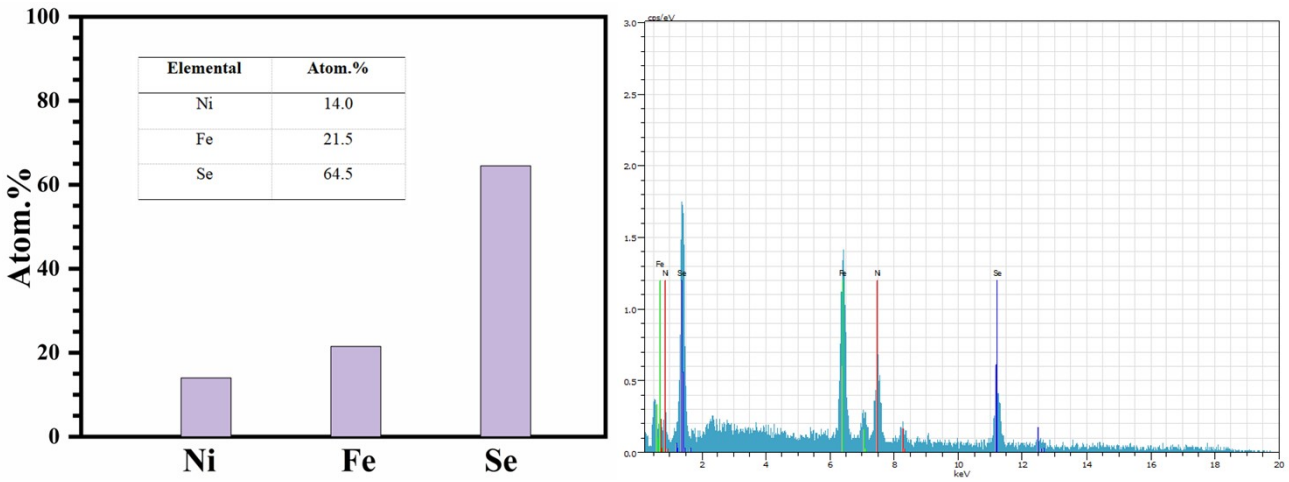

Figure S5. The atomic percentage of the element contents of the centrifugation precipitate.

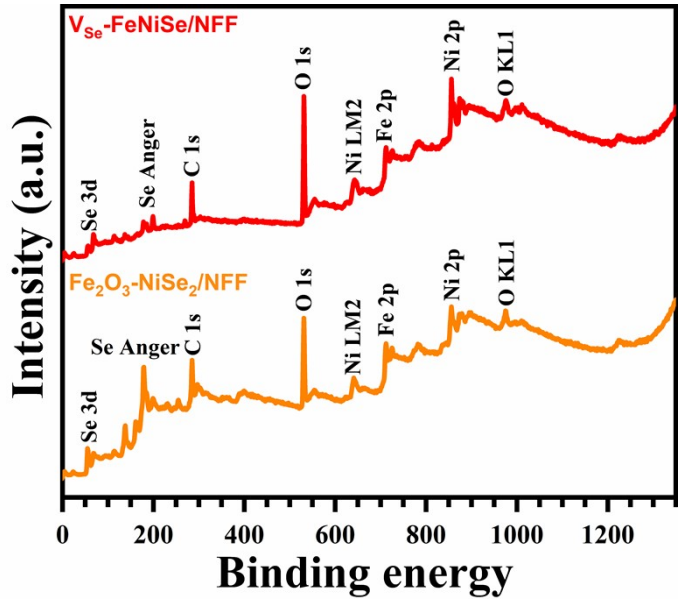

Figure S6. XPS overall spectrum of Fe_2O_3-$NiSe_2$/NFF and V_{Se}-FeNiSe/NFF in high-resolution.

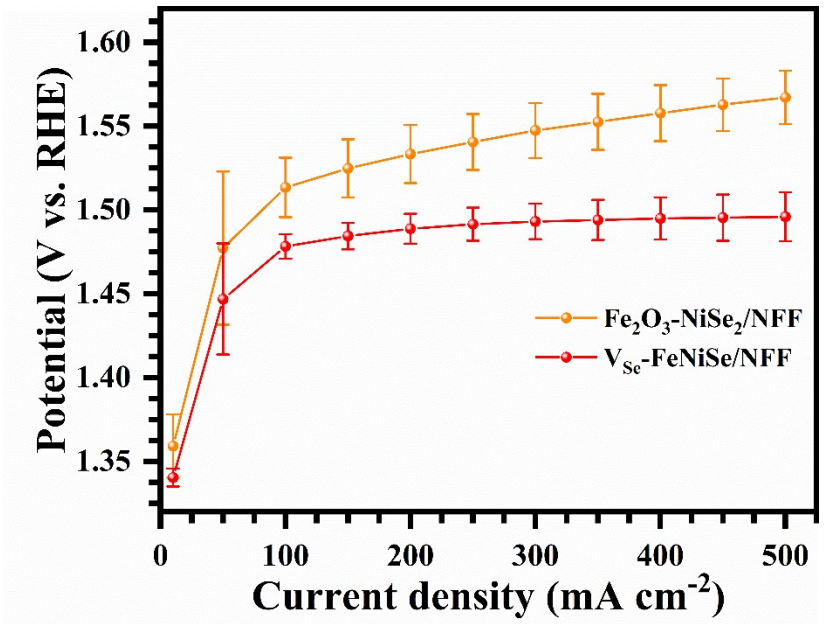

Figure S7. The performance error bar chart of Fe_2O_3-$NiSe_2$/NFF and V_{Se}-FeNiSe/NFF.

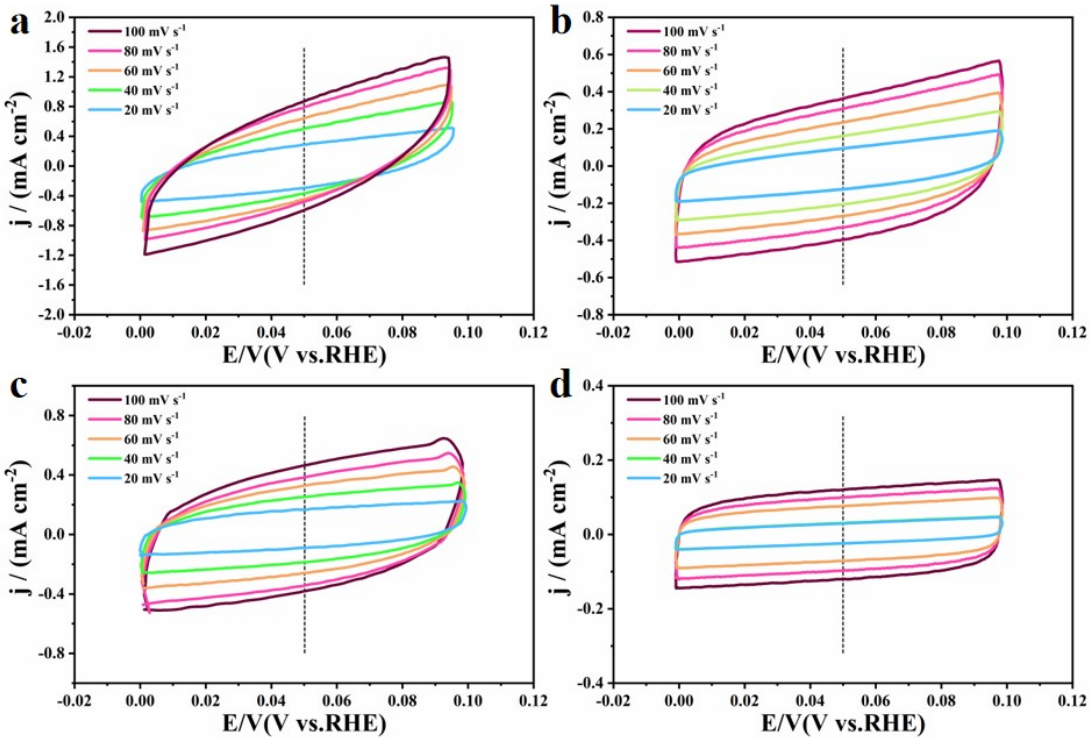

Figure S8. Cyclic voltammograms curves of (a) V_{Se}-FeNiSe/NFF, (b) Fe_2O_3-$NiSe_2$/NFF, (c) RuO_2/NFF and (d) NFF at different scan rates from 20 to 100 mV s^{-1}.

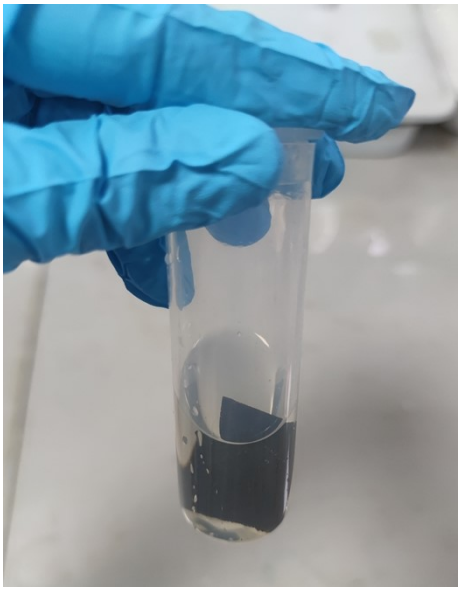

Figure S9. The macroscopic photographs of solutions after sonication of V_{Se}-FeNiSe/NFF for 4 h.

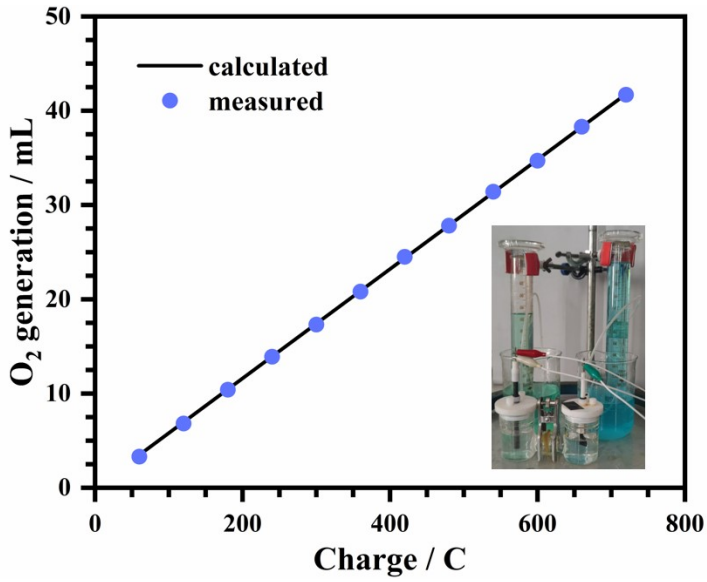

Figure S10. Determination of the Faradaic efficiency and its device for the V_{Se}-FeNiSe/NFF electrode during water electrolysis at a fixed current density of 100 mA cm^{-2} in a 1.0 M KOH electrolyte solution.

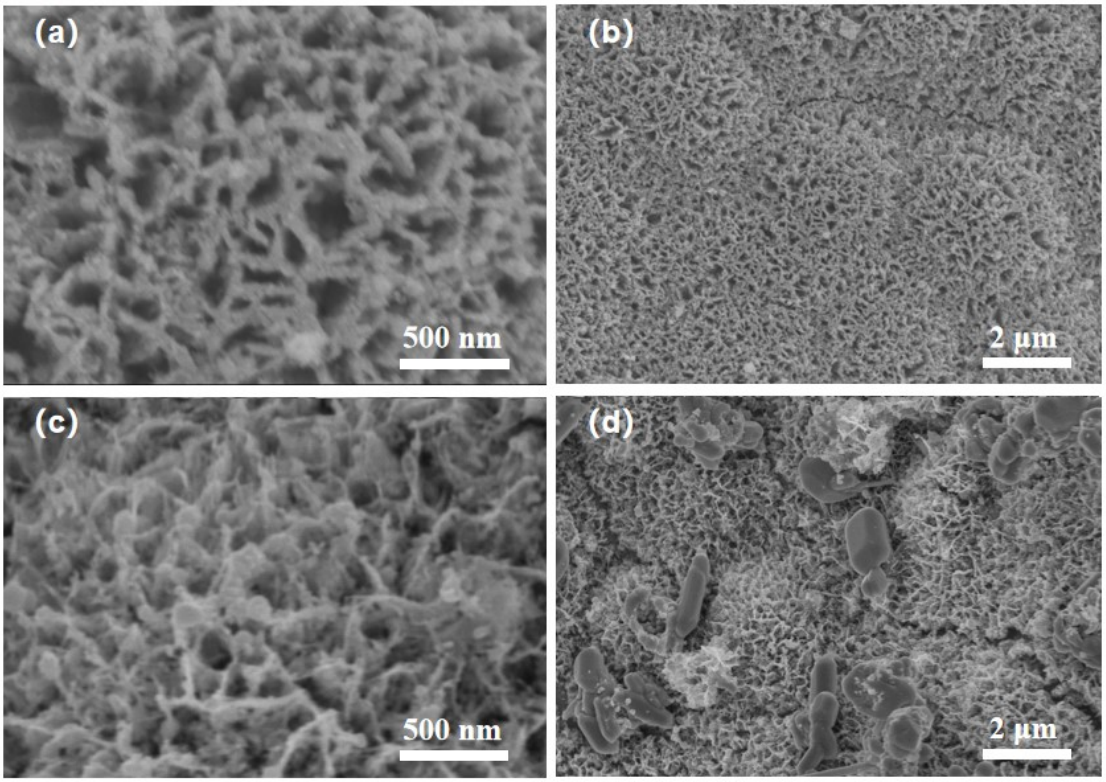

Figure S11. SEM images of Fe_2O_3-$NiSe_2$/NFF at different hydrothermal times: (a, b) 9 h, (c, d) 15 h.

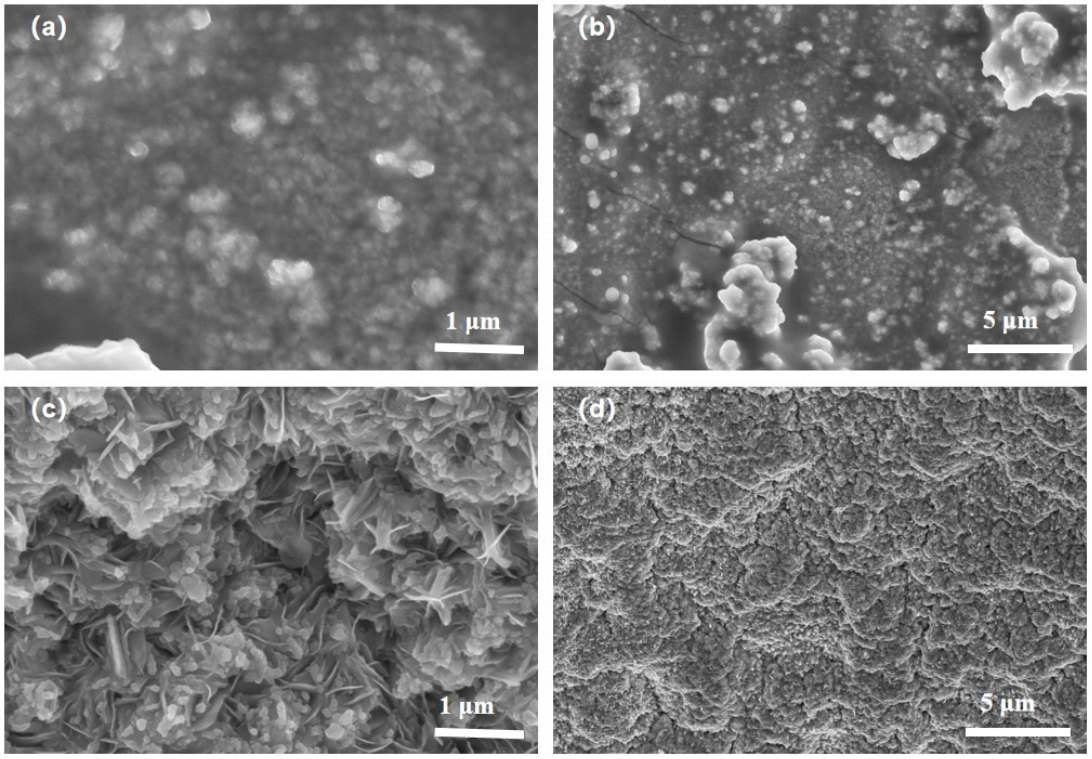

Figure S12. SEM images of Fe_2O_3-$NiSe_2$/NFF prepared at different hydrothermal temperature: (a, b) 90 °C, (c, d) 150 °C

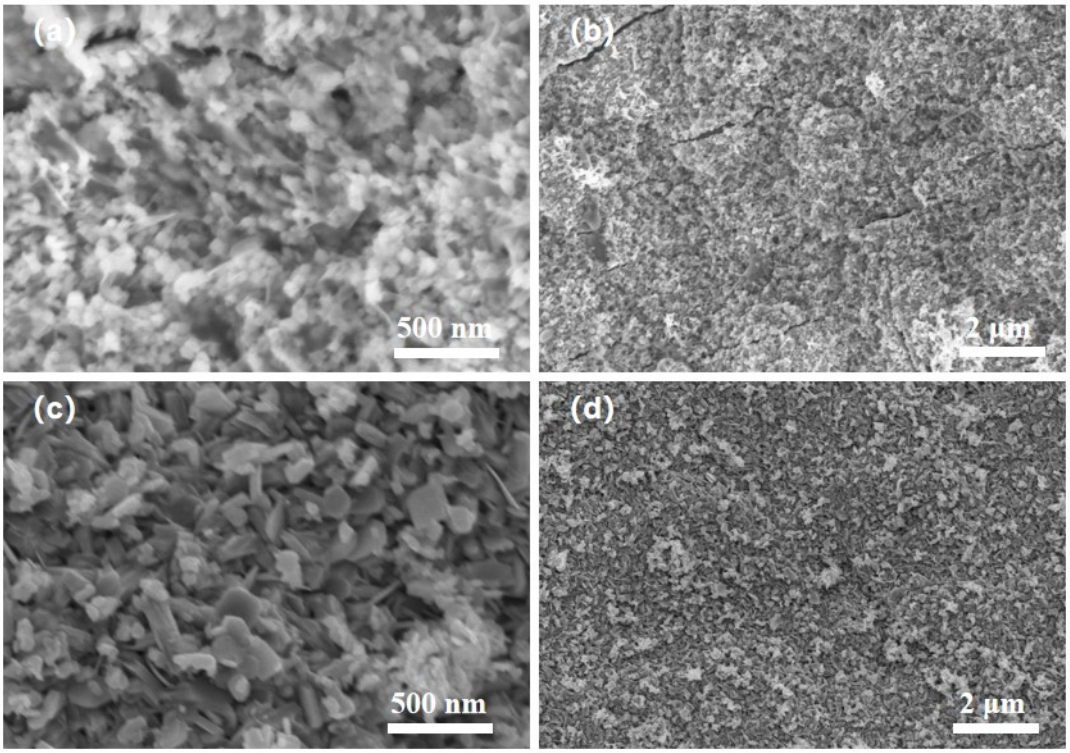

Figure S13. SEM images of the samples obtained using different reagent concentration: (a, b) 0.02 mmol, (c, d) 0.1 mmol.

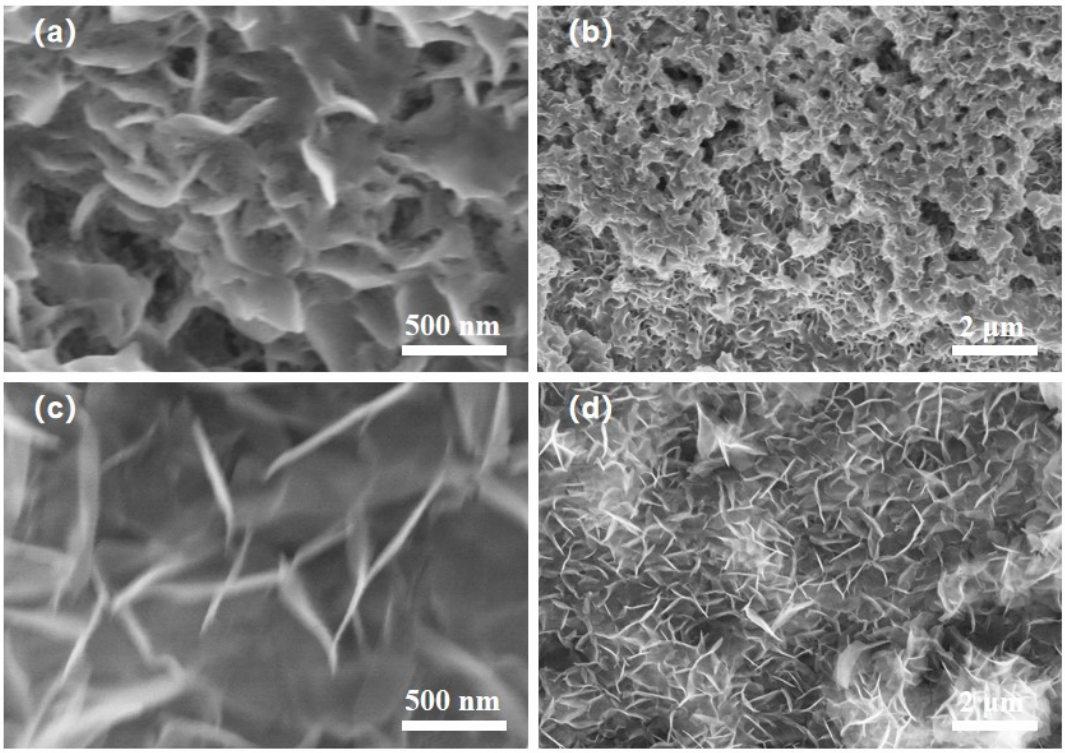

Figure S14. SEM images of V_{Se}-FeNiSe/NFF at different etching times: (a, b) 15 min, (c,d) 45 min.

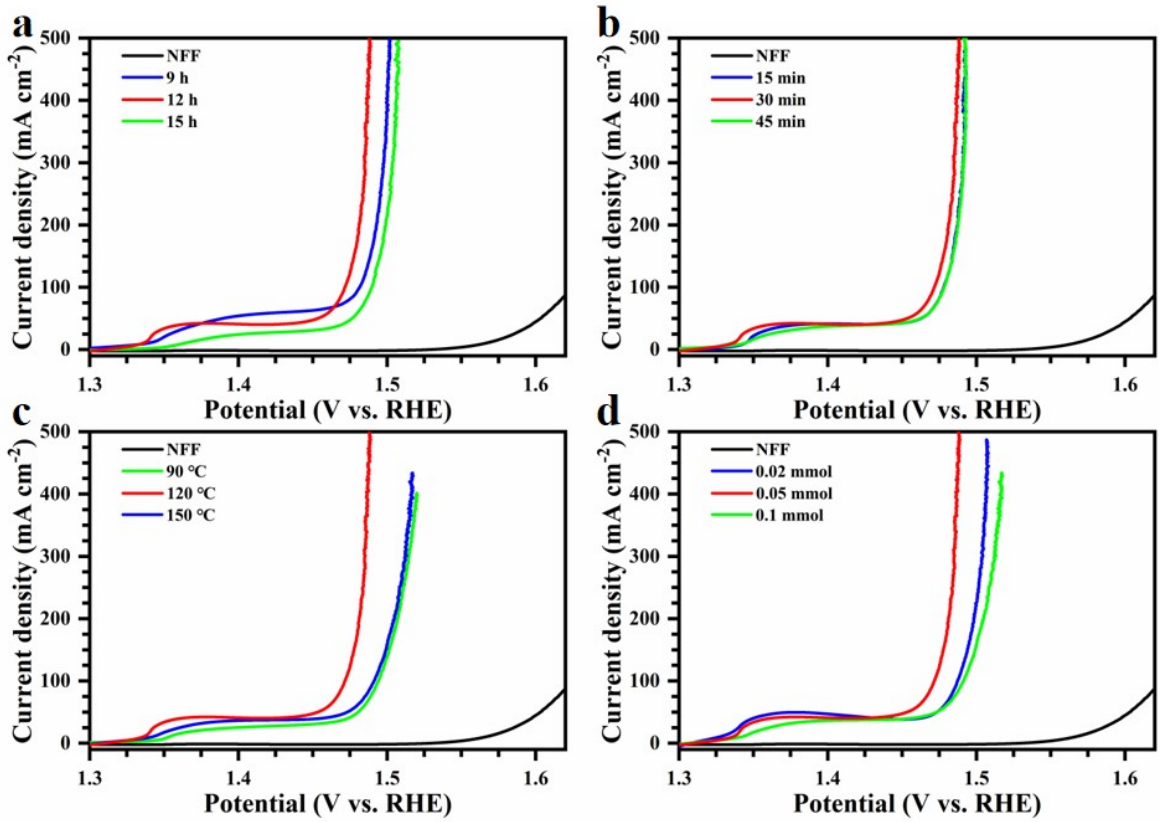

Figure S15. LSV curves at different preparation conditions: (a) Different hydrothermal times; (b) Different etching times; (c) Different hydrothermal temperatures; and (d) Different reagent concentration.

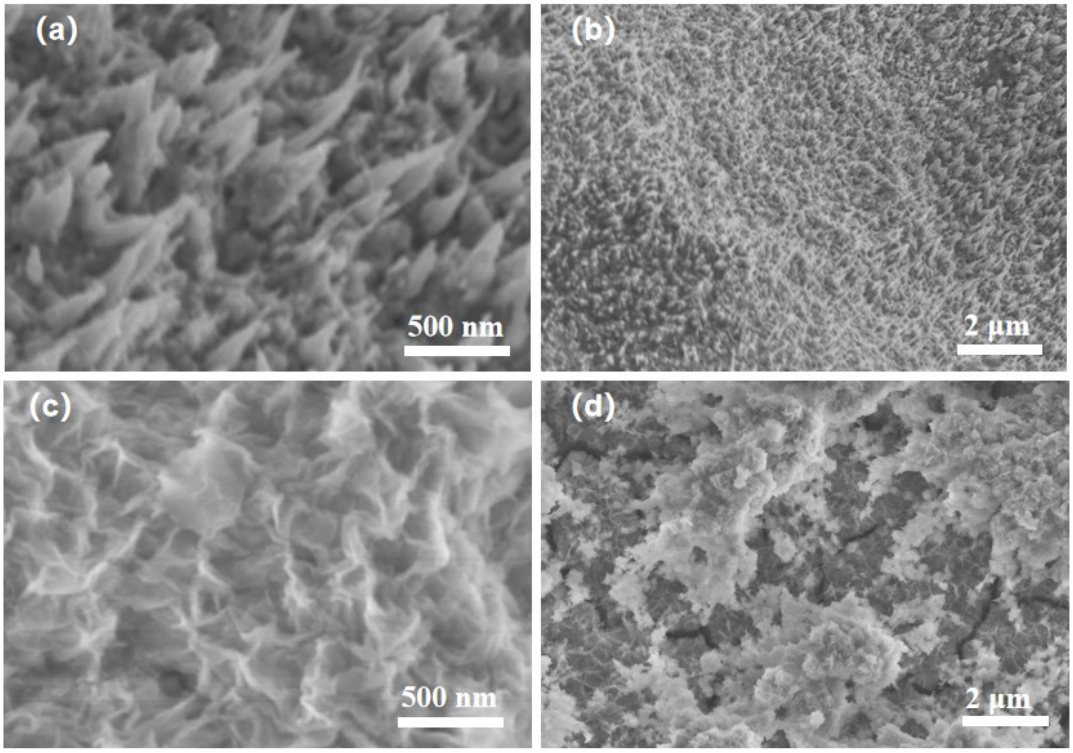

Figure S16. SEM images of the samples fabricated at the same conditions of Fe_2O_3-$NiSe_2$/NFF and V_{Se}-FeNiSe/NFF except for the NF as the substrate, (a, b) Before etching, named as NiSe/NF, (c, d) Etching treatment, named as E-NiSe/NF.

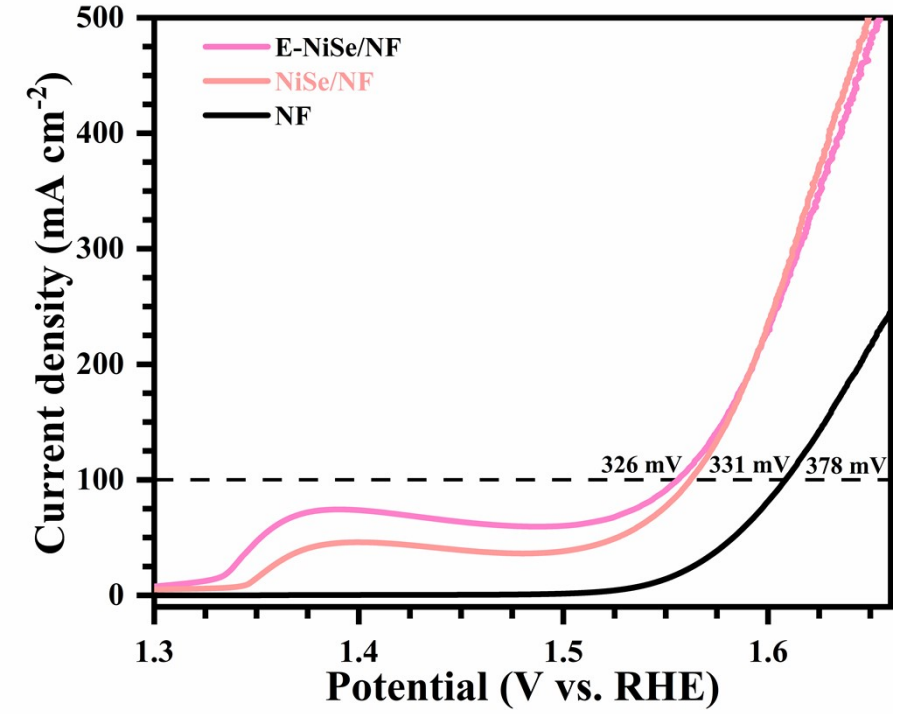

Figure S17. LSV curves of NF, NiSe/NF and E-NiSe/NF.

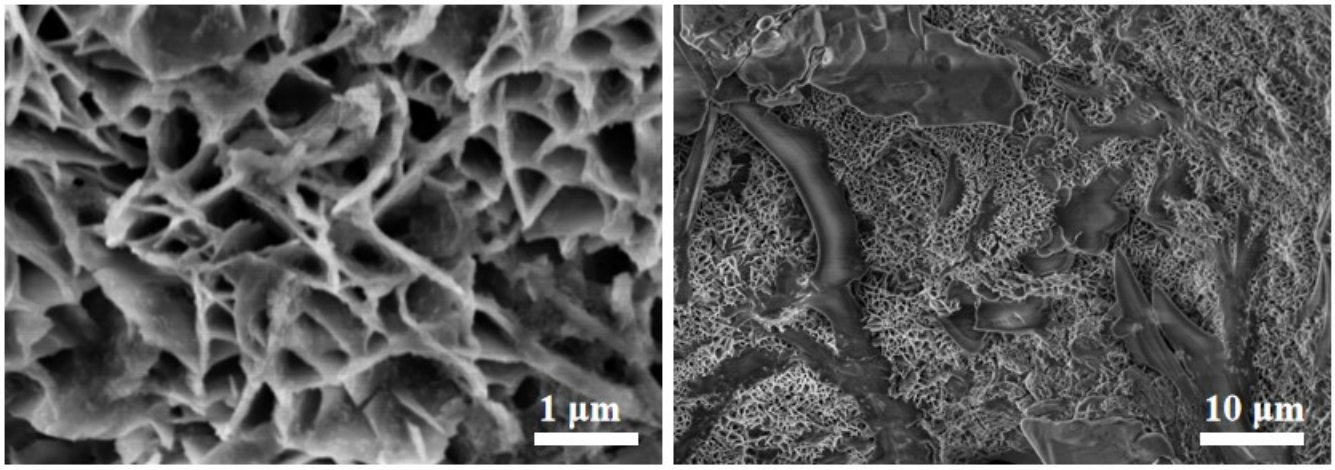

Figure S18. SEM images of V_{Se}-FeNiSe/NFF after OER testing for 100 h in seawater.

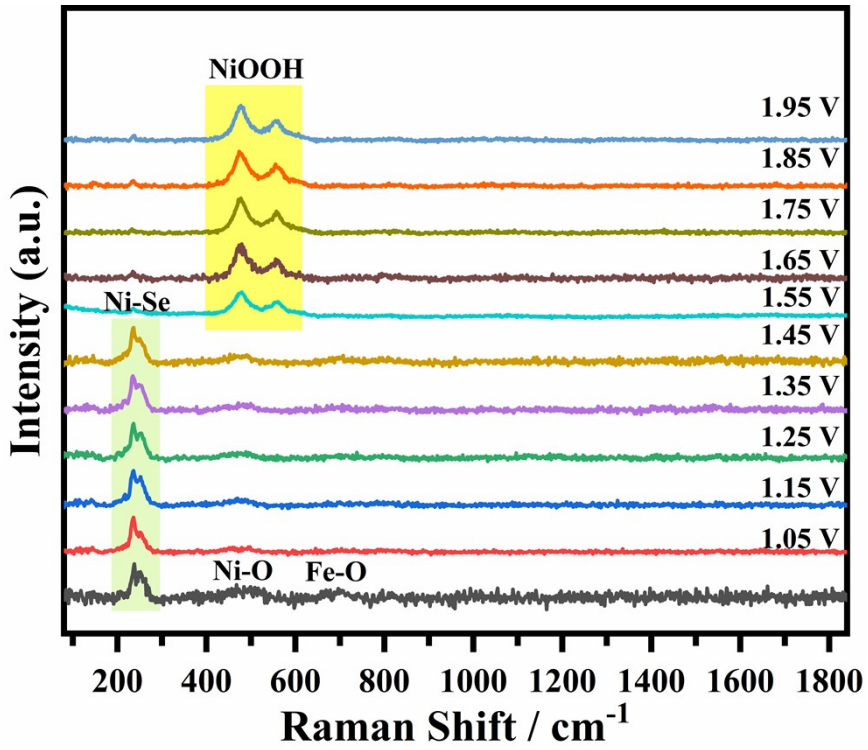

Figure 19. In situ Raman spectra of Fe_2O_3-$NiSe_2$/NFF in 1 M KOH.

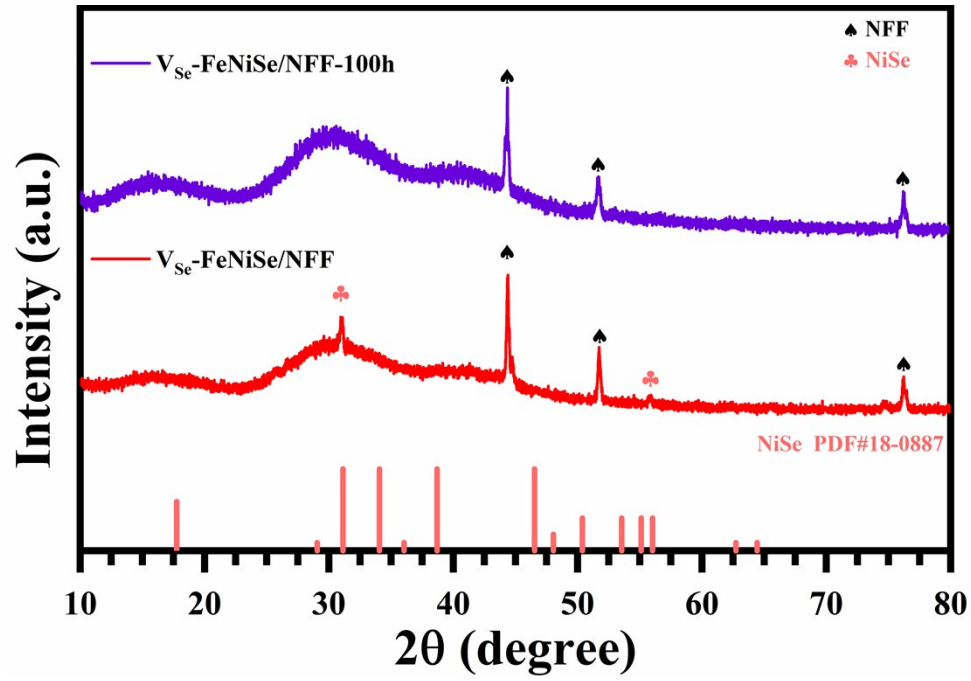

Figure S20. The XRD patterns of V_{Se}-FeNiSe/NFF before and after OER test for 100 h.

Table S1. Comparison of the overpotential and Tafel slope of V_{Se}-FeNiSe/NFF with reported Ni/Fe-based catalysts in alkaline

Catalyst	Overpotential (mV)	Tafel (mV dec^{-1})	References
V_{Se}-FeNiSe/NFF	242	30	This work
Fe_2O_3-$NiSe_2$/NFF	271	50.4	This work
NiFeV/NF	263	33	[1]
Fe,P-$NiSe_2$	266	39.5	[2]
P-(Ni,Fe)OxHy	251	25.1	[3]
Ni_2P-Fe_2P/NF	261	58	[4]
Co-FeP	274	57	[5]
$Co_{0.4}Ni_{1.6}P$ – CeO_2/NF	343	79.3	[6]
R-CoNiPS	300	37	[7]
Ni_2P@$NiMoO_4$/NF	264	35.21	[8]
CoFeOF/NF	280	46.35	[9]
Ni@CNTs–MoxC/Ni_2P	297	71	[10]
BZ-NiFe-LDH	230	45.05	[11]
(NiFeCoV)S_2	220	49.51	[12]
Fe1-Ni_3S_2/NF	244	50	[13]
Nix-Fe_3N@NCPs	249	42.8	[14]
D-NiFeV-LDHs	248	43.2	[15]
NiMoS@NSC	307	44.18	[16]
RuSA-NiS_2-FeS_2	304	64.2	[17]

Table S2. Comparison of overpotential and Tafel slope of each catalyst at a current density of 100 mA cm^{-2} in Seawater.

Catalysts	Overpotentials (mV)	Tafel (mV dec^{-1})	References
V_{Se}-FeNiSe/NFF	253	35.5	This work
Fe_2O_3-$NiSe_2$/NFF	284	62.2	This work
S-$NiFeSe_2$	367	32	18
Fe-$NiSe_2$ NFs	266	39.5	2
CoS_2@CoFe-LDH	358	79	19
NNNF@Mo_2N/FeO_xN_y	348	345	20
Se_{25}-NiTe/NF	345	34	21
CoFeOF/NF	280	51.98	9
Ni_2P@$NiMoO_4$/NF	292	45.95	8
NF/$(CoMo)_{0.85}$Se@FeOOH	287	52.5	22
BZ-NiFe-LDH	300	/	11
S-FeNi@NF	330	141	23
Fe1-Ni_3S_2/NF	306	80	13
NiFe@DG	276	39.7	24
NiFe LDH/Ni_3S_2	268	43.5	25
$Co_2(OH)_3Cl$	368	58.5	26

Reference

1. M. Qi, M. Qin, H. Wang, B. Lin, J. Chen, X. Shi, X. Du, S. Mao, J. Zhao, H. Zhang, L. Xi and Y. Wang, *App. Catal. B,* 2024, **356**, 124259.
2. J. Chang, G. Wang, Z. Yang, B. Li, Q. Wang, R. Kuliiev, N. Orlovskaya, M. Gu, Y. Du, G. Wang and Y. Yang, *Adv. Mater.*, 2021, **33**, 2101425.
3. Z. Zhu, X. Yang, J. Liu, M. Zhu and X. Xu, *Carbon Energy*, 2023, **5**, e327.
4. L. Wu, L. Yu, F. Zhang, B. McElhenny, D. Luo, A. Karim, S. Chen and Z. Ren, *Adv. Funct. Mater.*, 2021, **31**, 2006484.
5. S. Wang, P. Yang, X. Sun, H. Xing, J. Hu, P. Chen, Z. Cui, W. Zhu and Z. Ma, *App. Catal. B*, 2021, **297**, 120386.
6. Y. Cong, X. Chen, Y. Mei, J. Ye and T.-T. Li, *Dalton Trans.*, 2022, **51**, 2923-2931.
7. F. Luo, P. Yu, J. Xiang, J. Jiang and S. Chen, *J. Energy Chem.*, 2024, **94**, 508-516.
8. X. Guo, X. He, X. Liu, S. Sun, H. Sun, K. Dong, T. Li, Y. Yao, T. Xie, D. Zheng, Y. Luo, J. Chen, Q. Liu, L. Li, W. Chu, Z. Jiang, X. Sun and B. Tang, *Small*, 2024, **20**, 2400141.
9. S. A. Patil, A. C. Khot, V. D. Chavan, I. Rabani, D.-k. Kim, J. Jung, H. Im and N. K. Shrestha, *Chem. Eng. J.*, 2024, **480**, 146545.
10. J. Wang, D. T. Tran, K. Chang, S. Prabhakaran, J. Zhao, D. H. Kim, N. H. Kim and J. H. Lee, *Nano Energy*, 2023, **111**, 108440.
11. L. Zhang, J. Liang, L. Yue, K. Dong, J. Li, D. Zhao, Z. Li, S. Sun, Y. Luo, Q. Liu, G. Cui, A. Ali Alshehri, X. Guo and X. Sun, *Nano Res. Energy*, 2022, **1**, 9120028.
12. C. Feng, M. Chen, Y. Zhou, Z. Xie, X. Li, P. Xiaokaiti, Y. Kansha, A. Abudula and G. Guan, *J. Colloid Interface Sci.*, 2023, **645**, 724-734.
13. Y. Bao, Z. Wu, B. Liu, K. Zhong, M. Guo, J. Tu, B. Wang and X. Lai, *ACS Appl. Nano Mater.*, 2023, **6**, 4360-4369.
14. G. Wang, W. Tang, Y. Chen, P. Ji, M. Lu, H. Wei, L. Cui, X. Chen and G. Wang, *Adv. Funct. Mater.*, 2024, **n/a**, 2404470.
15. H. Li, Q. Yu, X. Zhu, H. Wu, Z. Dai, L. Li, W. Zhu, S. Li and Z. Chen, *Chem. Eng. J.*, 2024, **493**, 152860.
16. X. Fan, B. Li, C. Zhu, F. Yan, X. Zhang and Y. Chen, *Small*, 2024, **20**, 2309655.
17. R. B. Ghising, U. N. Pan, M. R. Kandel, P. P. Dhakal, S. Sidra, D. H. Kim, N. H. Kim and J. H. Lee, *J. Mater. Chem. A*, 2024, **12**, 3489-3500.
18. X. Chen, Y. Yu, X. Han, H. Wang, Y. Hua, D. Wu, P. Deng, J. Xiao, X. Tian and J. Li, *Sci. China Chem.*, 2024, **67**, 2747-2754.
19. G. Afshan, S. Karim, Y. P. Kharwar, T. Aziz, S. Saha, S. Roy and A. Dutta, *Small*, 2024, **n/a**, 2406431.
20. Y. He, Y. Hu, Z. Zhu, J. Li, Y. Huang, S. Zhang, M. S. Balogun and Y. Tong, *Chem. Eng. J.*, 2024, **489**, 151348.
21. H. Tan, Z. Yu, A. P. LaGrow, S. Ma, J. Wang, H. Li, D. Xiong and L. Liu, *J. Mater. Chem. A*, 2023, **11**, 26152-26163.
22. P. Li, S. Zhao, Y. Huang, Q. Huang, Y. Yang and H. Yang, *ACS Catal.*, 2023, **13**, 15360-15374.
23. T. Jia, X. Li, Z. Lin, H. Wang, K. Zong, P. Chen, C. Li, L. Li, D. Wang, L. Chen and S. Li, *J. Alloys Compd.*, 2024, **983**, 173792.
24. Z. Gong, J. Liu, M. Yan, H. Gong, G. Ye and H. Fei, *ACS Nano*, 2023, **17**, 18372-18381.
25. Z.-H. Zhang, Z.-R. Yu, Y. Zhang, A. Barras, A. Addad, P. Roussel, L.-C. Tang, M. Naushad, S. Szunerits and R. Boukherroub, *J. Mater. Chem. A*, 2023, **11**, 19578-19590.
26. L. Zhuang, J. Li, K. Wang, Z. Li, M. Zhu and Z. Xu, *Adv. Funct. Mater.*, 2022, **32**, 2201127.